



Unobstructed electron transfer on porous polyelectrolyte nanostructures and its characterization by electrochemical surface plasmon resonance

Bryce W. Davis, Matthew J. Linman, Kamara S. Linley, Christopher D. Hare, Quan Cheng*

Department of Chemistry, University of California, Riverside, CA 92521, United States

ARTICLE INFO

Article history:

Received 13 October 2009

Received in revised form 24 February 2010

Accepted 27 February 2010

Available online 7 March 2010

Keywords:

Polyelectrolyte

Surface plasmon resonance

Electrochemical SPR

Layer-by-layer deposition

ABSTRACT

Thin organic films with desirable redox properties have long been sought in biosensor research. We report here the development of a polymer thin film interface with well-defined hierarchical nanostructure and electrochemical behavior, and its characterization by electrochemical surface plasmon resonance (ESPR) spectroscopy. The nano-architecture build-up is monitored in real time with SPR, while the redox response is characterized by cyclic voltammetry in the same flow cell. The multilayer assembly is built on a self-assembled monolayer (SAM) of 1:1 (molar ratio) 11-ferrocenyl-1-undecanethiolate (FUT) and mercaptoundecanoic acid (MUA), and constructed using a layer-by-layer deposition of cationic poly(allylamine hydrochloride) (PAH) and anionic poly(sodium 4-styrenesulfonate) (PSS). Electron transfer (ET) on the mixed surface and the effect of the layer structures on ET are systematically studied. Under careful control, multiple layers can be deposited onto the 1:1 FUT/MUA SAM that presents unobstructed redox chemistry, indicating a highly ordered, extensively porous structure obtained under this condition. The use of SPR to trace the minute change during the electrochemical process offers neat characterization of local environment at the interface, in particular double layer region, allowing for better control over the redox functionality of the multilayers. The 1:1 SAM has a surface coverage of $4.1 \pm 0.3 \times 10^{-10} \text{ mol cm}^{-2}$ for ferrocene molecules and demonstrates unperturbed electrochemistry activity even in the presence of a 13 nm polymer film adhered to the electrode surface. This thin layer possesses some desirable properties similar to those on a SAM while presenting $\sim 15 \text{ nm}$ exceedingly porous structure for high loading capacity. The high porosity allows perchlorate to freely partition into the film, leading to high current density that is useful for sensitive electrochemical measurements.

© 2010 Elsevier Ltd. All rights reserved.

1. Introduction

Electroactive thin organic films have attracted much interest because of their wide range of applications as electro-optics, semiconductor devices, molecular memory electronics, electrochromic displays, and sensors [1–9]. A number of methods have been developed to create these ultrathin multilayer films, such as the Langmuir–Blodgett (LB) assembly, dip-coating, spin-coating, and vapor-deposition, among others [10–15]. Although the LB assembly technique offers a versatile way to build a functional surface at a liquid/gas interface, LB films must be formed in a very condensed manner to obtain proper film stability due to the weak nature of the non-covalent forces [16]. Dip-coating and spin-coating are commonly adopted techniques for achieving thin multilayer films because of simplicity, low cost, and efficiency of coverage. However, these approaches usually yield molecularly disordered structures, and are difficult to control and monitor at nanometer scale. Vapor-

deposition method is a useful technique for coating substrates with high purity and high performance metal oxides and semiconductors. Its use for depositing organic molecules is limited due to the required operational conditions of high temperature, vacuum and volatile precursors, and the formation of volatile by-products is a common result [17]. There is a need to explore alternatives to creating nanoscale 3D architecture that provides a more ordered surface with high quality and desirable features such as controlled porosity.

One attractive technique for building a 3D multilayer molecular nanostructure is the “layer-by-layer” (LbL) method, which works by alternating physisorption of oppositely charged molecules [18]. Many types of charged molecules and nano-objects are suitable for deposition by the LbL method, such as DNA, enzymes, viruses, and polyelectrolytes [19–22]. One advantage of the LbL method is that the amount of material deposited on each cycle approaches a constant and reproducible value, allowing a large number of controllable layers and specific properties to be incorporated into the thin films. The initial layer on the substrate is important for the functionality of the nanostructure and a versatile technique to achieve this first layer is self-assembled monolayers (SAMs). SAMs provide a convenient, flexible, and straightforward system

* Corresponding author. Tel.: +1 951 827 2702; fax: +1 951 827 4713.
E-mail address: quan.cheng@ucr.edu (Q. Cheng).

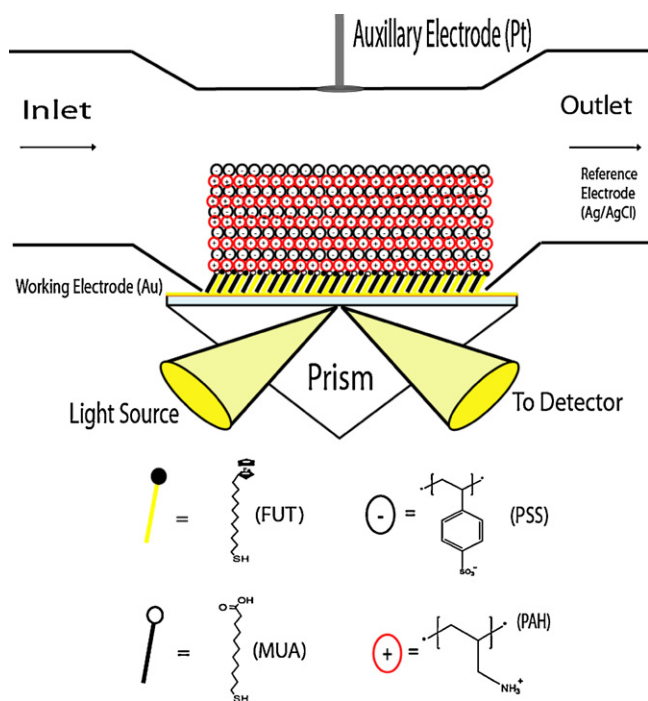


Fig. 1. A schematic of LbL build-up of polymeric thin films on a mixed SAM with ESPR configuration and structure of polyelectrolytes and alkythiol derivatives for self-assembly.

with which to tailor the interfacial properties of organic functional groups and metal oxides [23–25]. The combination of LbL and SAMs is a great bottom-up approach to creating a functionally active nanostructure.

Many methods have been used to analyze the build-up of these molecular structures on a solid substrate, such as ellipsometry, atomic force microscopy (AFM), cyclic voltammetry (CV), and surface plasmon resonance (SPR) spectroscopy. The combination of electrochemistry and SPR is of particular interest to us due to its ability to probe the interface properties simultaneously on two different physical quantities at the same surface inside an electrochemical cell [26–28]. Cyclic voltammetry in particular offers kinetic measurement of heterogeneous electron-transfer reactions and coupled chemical reactions [29,30]. SPR, a direct optical-sensing technique, measures the refractive index change due to specific interactions occurring at a metal dielectric interface [31,32]. The use of SPR to monitor the creation of multilayer films is advantageous because one could promptly observe film thickness change and screen for new polymers in real time with no external/internal labels using only small volumes of sample. Application of electrochemical surface plasmon resonance (ESPR) for monitoring the development of polymeric film build-up while simultaneously examining redox characteristics has appeared in a few recent publications [33–35].

In this work, we report the development of a polymer thin film interface with well-defined hierarchical nanostructure and electrochemical behavior, and its characterization by ESPR spectroscopy. Our focus is to build nano-architectures less than 20 nm in thickness that offer higher loading capacity while still exhibiting attractive physiochemical (redox in this case) properties as those observed on a 2 nm alkythiol homogeneous monolayer. Thin films of these characteristics are very useful for creation of energy-efficient miniaturized devices and biosensors, but have not been widely studied largely due to lack of proper fabrication methods. Fig. 1 illustrates the scheme of the design and the structure of the SAMs and polyelectrolytes utilized in this work. A mixed

SAM surface of 11-ferrocenyl-1-undecanethiol (FUT) and mercaptoundecanoic acid (MUA) is used, which lends itself to two different primary functions. The ferrocene surface provides electrochemical signal while the carboxylic acid will allow for a more desirable electrostatic attachment for the polyelectrolytes. Specifically we plan to seek to achieve 3D nano-architecture with properties matching those on 2D surfaces in terms of efficient ET with a bottom-up approach. A facile redox communication is sought to take place after organic layers are coated to the surface. We will also take advantage of the high sensitivity of SPR to explore the doping and dedoping process on the thin films, in an attempt to understand and optimize the ion mobility property across the membrane.

2. Experimental

2.1. Materials

Poly(sodium 4-styrenesulfonate) (PSS), poly(allylamine hydrochloride) (PAH), mercaptoundecanoic acid (MUA) and NaClO_4 were purchased from Aldrich (Milwaukee, WI). Dojindo Molecular Technologies (Japan) supplied the 11-ferrocenyl-1-undecanethiol (FUT). Microscope slides were purchased from Fisher (Pittsburgh, PA) and the platinum wire (0.5 mm, 99.997%) was purchased from Alfa Aesar (Ward Hill, MA). All chemicals were of the highest analytical grade, and were used without further purification. Milli-Q (>18 M Ω) water was used in the preparation of all electrolyte solutions, and absolute ethanol was used to prepare all thiol solutions.

2.2. Preparation of redox active self-assembled monolayer electrodes

The Au electrodes were prepared by e-beam evaporation of a thin film of Au (ca. 46 nm) onto microscope glass slides with 2-nm Cr as the adhesive layer. Prior to modification, the Au substrates were cleaned with piranha solution, then extensively rinsed in Milli-Q water, absolute ethanol, and dried with a stream of N_2 gas. The electrodes were then immersed in a 1 mM (1:1) FUT/MUA for 12–24 h and rinsed with ethanol, DI water and dried in a N_2 stream. The same procedure was repeated for all other SAM surfaces used in this work.

2.3. Cyclic voltammetry

The electrochemical measurements were carried out with a three-electrode system using a CHI 650 electrochemical work station (CH Instruments, Austin, TX). The modified Au electrode served as the working electrode, and an Ag/AgCl electrode was used as the reference electrode which was placed at the outlet of the nanoSPR flow cell. The platinum counter electrode was machined into the top of the SPR flow cell. The 0.1 M NaClO_4 (pH 6.6) solution was used as the supporting electrolyte. The CV data fitting was performed using Origin software (Microcal, Inc.). The quantity of electro generated ferrocenium (Γ_{Fc^+}) was calculated using the following equation (Eq. (1)) [36]:

$$\Gamma_{\text{Fc}^+} = \frac{Q_{\text{Fc}^+}}{nFA} \quad (1)$$

where Q_{Fc^+} is the charge associated with the ferrocene oxidation determined through the integration of the voltammetric anodic peak corrected for the charging current, n is the number of electrons involved in the electron-transfer process ($n=1$ for the ferrocene redox couple), F is the Faraday constant, and A is the geometric surface area of the exposed FUT/MUA substrate electrode, which is defined by a silicon rubber cast.

2.4. Surface plasmon resonance

The surface plasmon resonance (SPR) spectrometer employed in the procedure is a dual channel nanoSPR in the Kretschmann configuration (Morton Grove, IL) with a semiconductor laser ($\lambda = 670$ nm) as the excitation source. Surface interaction and modification were monitored and characterized using the tracking mode of SPR angular scanning at the minimum angle. The SAM modified working electrodes were clamped down to a flow cell on a high-refractive index prism (Fig. 1). Once the electrolyte solution had established a stable baseline, 1 mg mL⁻¹ of PAH and PSS (in 0.1 M NaClO₄) were injected in sequential order for layer build-up.

2.5. Atomic force microscopy (AFM)

AFM images were obtained using a Veeco Dimension 5000 atomic force microscope (Santa Barbara, CA) with manufacturer provided software. All images were obtained under the tapping mode, and root-mean-square (rms) surface roughness values were obtained by averaging multiple 25 μm^2 areas across the entire surface area at a scan rate of 1.5 Hz.

2.6. Ellipsometry measurements

Spectroscopic ellipsometric (SE) measurements were conducted using a Jobin Yvon UVISSEL (Edison, NJ) Spectroscopic Phase Modulated Ellipsometer (SPME) Version M200 in the spectral range of 300–800 nm. For all SE measurements, the chip was placed on a sample stage situated on a goniometer with light from a 75W Xenon arc source at 70° angle of incidence, and reflected light was detected by a PMT. Three spots on each substrate surface were analyzed, and the results were averaged. The thickness of the FUT/MUA monolayer and the subsequent polymer layers was determined from using the Levenberg–Marquardt non-linear optimization algorithm within the vendor's DeltaPsi2 software. The thickness of the chromium and gold were fixed to the measured thickness during the calibrated quartz crystal monitor during e-beam evaporation (2 and 46 nm, respectively). The $n(\lambda)$ and $k(\lambda)$ values provided in the vendor's materials database for gold, polycrystalline chromium, and BK7 glass were used in the fitting process. For the FUT/MUA monolayer, the refractive index (n) used were $n = 1.464$ [26,37] and $n = 1.45$ [38], respectively. The n value used for the polyelectrolytes was $n = 1.54$ [39,40]. The extinction coefficient (k) for all polymers in the calculations was set to be $k = 0$ [41].

3. Results and discussion

3.1. Electrochemical behavior of FUT/MUA interface

Ferrocenylalkanethiolate SAMs are a much studied electroactive system, and their Faradic electrochemistry is extensively documented [26,42–46]. Fig. 2 shows a cyclic voltammogram of a well-defined reversible redox wave for 1:1 mixture of FUT/MUA (curve 1) and a flat wave for MUA (curve 2) in 0.1 M NaClO₄. Symmetrical redox peaks were obtained with a slight peak separation at a scan rate of 100 mV s⁻¹. The oxidation, reduction and formal potential (E°) of the terminal ferrocene group in the monolayer were found to be 412, 382 and 397 mV, respectively. A peak separation (ΔE_p) of 30 mV is a strong indicator that a facile electrochemical process occurs on the electrode surface. The coverage of FUT, from the charge of the anodic peak (45 $\mu\text{C cm}^{-2}$), is calculated to be 4.7×10^{-10} mol cm⁻². The CV shown in Fig. 2 and the data reported compare well to values previously reported in the literature [26,42,45]. To screen for the most suited electrolyte for this work, solutions of 0.1 M HClO₄, LiClO₄, and NaClO₄ were tested.

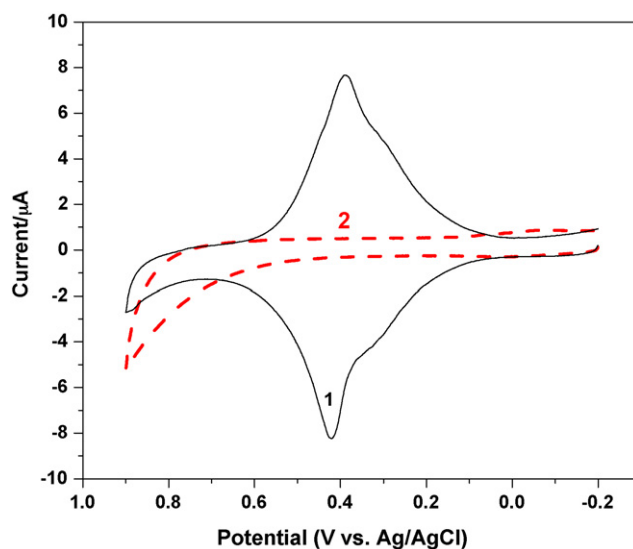


Fig. 2. Cyclic voltammograms for MUA (curve 1) and 1:1 FUT/MUA (curve 2) in 0.1 M NaClO₄ (pH 6.6). The scan rate is 100 mV s⁻¹.

NaClO₄ offers the most consistent signal among the three, especially with polyelectrolytes, and has thus been used throughout the work.

It should be noted that a small shoulder peak is located on the negative potential side of the FUT/MUA response. In fact, this is a common trait found in ferrocene containing SAMs, and it is believed that the shoulder is due to the inhomogeneous spatial distribution of ferrocene in the SAM [26]. The shoulder peak was further examined by comparing the FUT/MUA SAM mixture with a pure FUT surface (supplementary material). As expected, the pure FUT SAM surface shows a larger current due to more ferrocene attached to the surface. However, the shoulder peak for the pure FUT SAM surface is also larger, indicating that mixed FUT/MUA SAMs can improve spatial distribution within the layer.

In order to perform an effective LbL build-up, the ratio of FUT to MUA was varied and optimized as it affects the negative surface charge density and thus the attachment of the polycations and redox current density. We compared the ratios of 1:10, 1:5, and 1:1 of FUT to MUA to screen for the optimal surface conditions and found that the 1:1 FUT/MUA surface gave the strongest and most reproducible redox communication at the same time achieving a high charge density (data not shown). This surface was chosen for further study and building of a 3D nanostructure with multiple layers.

3.2. Characterization of electrostatic self-assembly by SPR

Real time monitoring of assembly of a polycation–polyanion molecular film with bottom-up construction was carried out with SPR. Fig. 3 shows the sensorgrams for the process. The result clearly reveals the build-up of the film by alternating the injection of polyelectrolytes with the corresponding charge. Since the MUA film contains carboxylic acid headgroup, polycationic PAH solution was first injected. The inset of Fig. 3 illustrates the specificity of the PAH onto the surface while polyanionic PSS does not bind on FUT/MUA. The first layer of polycation adhesion produced a signal increase of 95 millidegrees. Once the baseline was stabilized, PSS was injected, giving an SPR angular increase of 200 millidegrees. PSS is a considerably larger molecule than PAH, therefore leading to a larger refractive index change and response in the SPR sensorgram. The electrostatic interaction between PAH and PSS is very effective and complete adsorption of the layers did not require any incubation

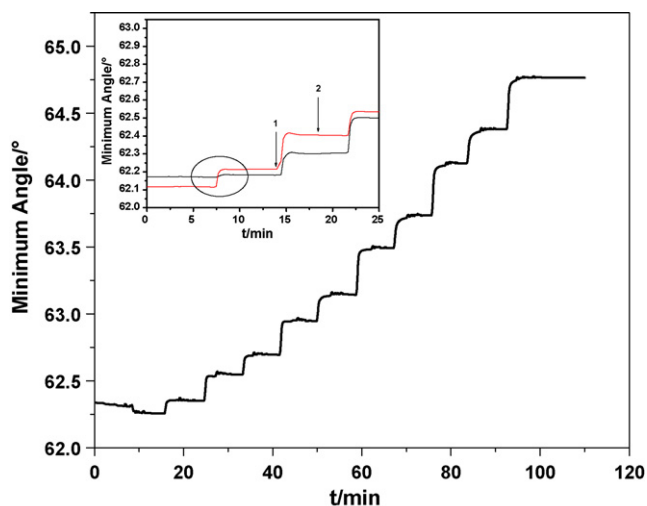


Fig. 3. SPR sensorgram of a 10-layer nanostructure build-up by alternating injection of oppositely charged polyelectrolytes in 0.1 M NaClO₄ on a 1:1 FUT/MUA SAM surface. Inset is an SPR sensorgram of a 5-layer build-up on a MUA surface. The circle illustrates the specific electrostatic interaction of PAH with surface carboxylate (red curve) while PSS (black curve) shows no interaction with the negatively charged surface. Arrows indicate first (1) and second (2) injection of the polyelectrolyte demonstrating complete adsorption of the polymer in the first injection.

time. For proof of principle all layers were injected twice. The second injection shows little signal as compared to the first injection, clearly demonstrating the completion of the electrostatic interaction right after the initial injection (Fig. 3). Flow rate was optimized at 138 $\mu\text{L}\cdot\text{min}^{-1}$, yielding a 10-layer nanoassembly in less than 100 min.

The pH-dependent thickness behavior of the sequentially adsorbed polyanions layers must be considered when creating multilayer thin films. Rubner et al. has studied the pH dependence properties extensively, demonstrating that control over the bulk and surface composition of the resulting multilayer films is readily achievable via simple pH adjustments [47,48]. Furthermore, pH controls the linear charge density of an adsorbing polymer as well as the charge density of the previously adsorbed polymer layer. In this work we focus on optimizing deposition solution at a relatively neutral pH for all polyanion adsorption for better control over the surface charge density and film thickness while at the same time offering high-quality voltammograms. We used 0.1 M NaClO₄ because it is a non-reactive electrolyte with a pH of ~ 6.6 , which in turn allowed for us to obtain controllable adsorption layers within the film.

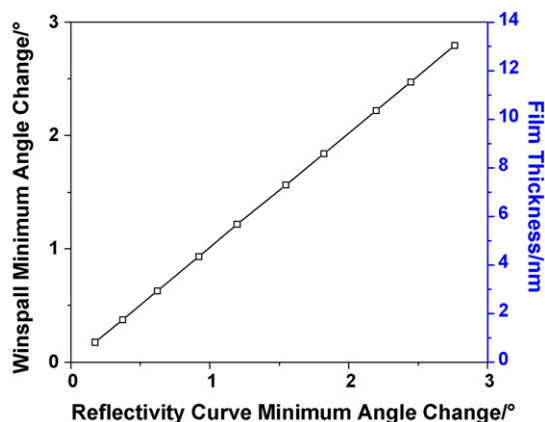
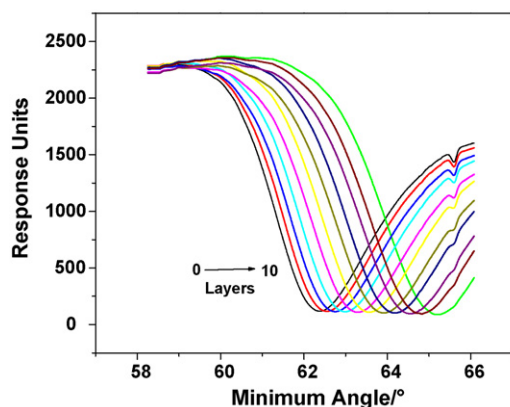


Fig. 4. SPR angular scan curves of reflectivity versus incident angle recorded after each layer of polyelectrolyte (left) and linear relationship between experimental and theoretical SPR minimum angle shifts for polymer films on SPR gold substrates (right).

A more careful study on the quantitative layer adding up has been performed with SPR and Fresnel simulation to understand the correlation of layer deposition and thickness increase. Fig. 4 shows a series of SPR angular scan curves of reflectivity versus incident angle recorded after each layer of polyelectrolyte was deposited. The left-most curve corresponds to the monolayer of FUT/MUA on the Au surface. A total of 10 layers of organic polyelectrolyte were added to the SAM surface, leading the reflection curves shifting from left to right. SPR angular shifts correlate very well with theoretical predictions from the Winspall program ($R^2 = 1$) developed by the Knoll group (Fig. 4 right). The average thickness of PAH and PSS is 0.96 and 1.2 nm, respectively. The overall thickness of the film is determined to be 12.6 nm, including the SAM surface.

3.3. Electrochemical behavior of the nanostructured multiple layers

To seek thin organic films exhibiting ideal electrochemical behavior, nanostructure of the FUT/MUA monolayer and polyelectrolyte multilayer were studied for their electron-transfer property. After the deposition of the polymer layers, it is expected that these layers block or slow down electron transfer because of the polymer attachment [49–51]. To our surprise, facile electron transfer can be achieved through the carefully prepared PAH/PSS thin films continuously. The physical stability of the electrode surface and polymer build-up appears to be good, with little to no deterioration after multiple scans. Fig. 5 shows the CV results on a 1:1 FUT/MUA SAM system with polymer deposition. The ferrocene on the FUT/MUA surface showed well-defined, reversible response after each layer was attached, suggesting the PAH/PSS films provide a favorable environment/membrane that does not interfere with the transfer of electrons and movement of counter ions. There is little or no effect on the magnitude and shape of the electrochemical signals even after the build-up of multiple layers of polymer. More detailed results are summarized in Table 1. The average current (i_p), peak separation (ΔE_p), and formal potential (E°) was found to be $8.6 \pm 0.3 \mu\text{A}$, $31 \pm 5 \text{ mV}$, and $398 \pm 2 \text{ mV}$ for all layers, respectively. The amount of adsorbed FUT remained constant at $4.7 \pm 0.9 \times 10^{-10} \text{ mol cm}^{-2}$, all of which strongly indicates there is unconstrained redox communication between the working electrode and the ferrocene interface even after adding 10 polymer layers.

Modified electroactive surfaces have been studied extensively. However, to sufficiently have facile counterion diffusion through a redox inactive film, efficient relay of electrons is often required within the film using redox active polymers [52]. Clearly effective ionic movement through the organic film above the redox SAM

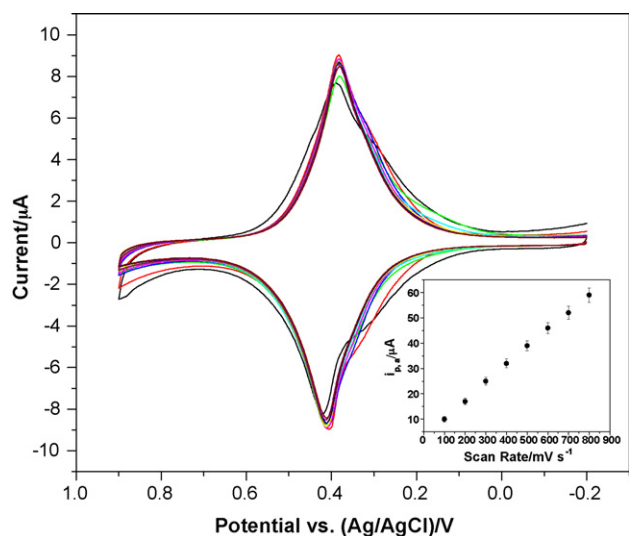


Fig. 5. Overlay of the cyclic voltammograms taken after each layer of polyelectrolyte was adsorbed on a 1:1 FUT/MUA surface in 0.1 M NaClO₄. The scan rate is 100 mV s⁻¹. Inset: The dependence of the *i_p* on the scan rate after each layer (*n* = 11).

plays an important role in the observed electrochemical properties [53,54]. To further understand the ionic movement, we evaluated the effect of scan rate on response. A plot of the average peak current versus the scan rate for all layers is shown in the insert of Fig. 5 with the appropriate error bars. The peak current (*i_p*) is directly proportional to the scan rate (*v*), not *v*^{1/2}, which is characteristic of ET for species immobilized on the surface of the electrode. Plotting log(*i_p*) versus log(*v*) yields an average slope of 0.92, which is slightly less than the anticipated value of 1.0 for surface-localized electroactive species. Nevertheless, this value is large and consistent with films of different thicknesses, further proving that the diffusion process of the non-electroactive species through the nanostructures is unhindered. We also observed the insensitivity of the average peak separation versus the scan rate up to 800 mV s⁻¹ for all layers, further illustrating an unobstructed mass transport through the film and facile electron tunneling at the surface (supplementary material). To our knowledge, this is the first report on unhindered redox chemistry through a 13 nm polyelectrolyte nanosystem without the use of a redox relay.

SPR is sensitive to the structural change on the Au surface, which offers a useful tool to probe continual functionalization of the nanoassembly. The electrochemical reaction of the ferrocene headgroup introduced a local change in the double layer zone and the result of this local change can cause an increase in refractive index. The ESPR technique employed here appears to be ideal to probe the changes within the dielectric layer from the applied

Table 1
Voltammetric results for peak current (*i_p*), formal potential (*E*^o), and peak separation (ΔE_p) obtained before and after each layer.

Layer	<i>i_p</i> , μA	<i>E</i> ^o , V	ΔE_p , mV
FUT/MUA	7.9	0.400	27
1	9.1	0.395	22
2	8.3	0.398	31
3	8.8	0.396	20
4	8.5	0.400	35
5	8.9	0.398	31
6	8.7	0.397	34
7	8.8	0.400	35
8	8.9	0.400	37
9	8.4	0.400	37
10	8.7	0.396	32

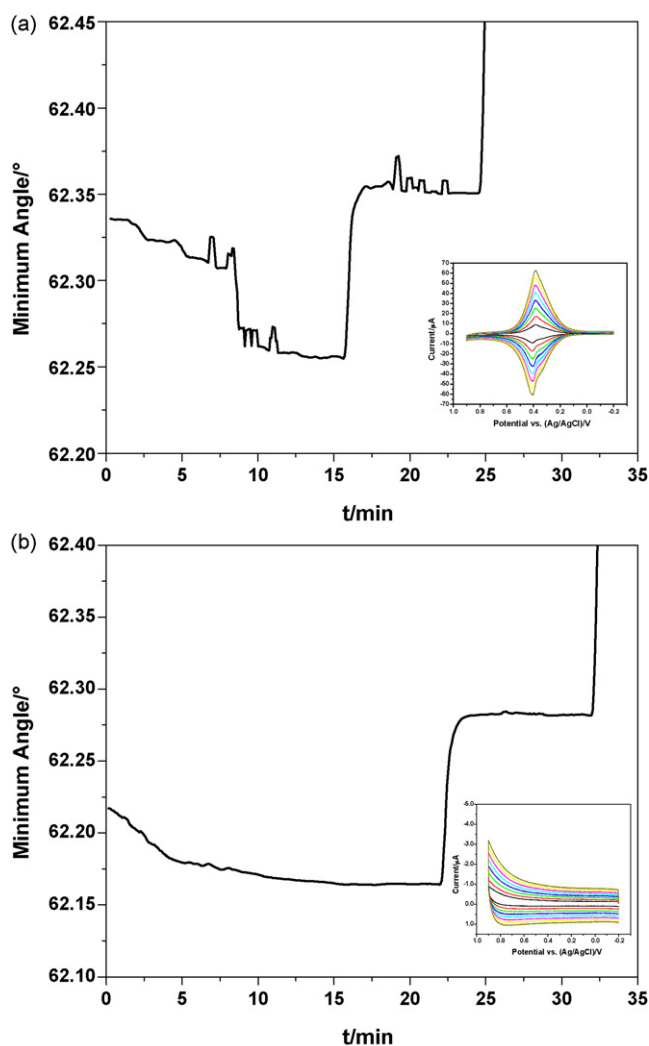


Fig. 6. (a) Zoomed-in SPR sensorgram of a 10-layer nanostructure on a 1:1 FUT/MUA SAM surface in a 0.1 M NaClO₄ solution. The spikes indicate SPR response to CV cycles. Inset is the overlay of cyclic voltammograms at different scan rates (100–800 mV). (b) Zoomed-in SPR sensorgram of a 10-layer nanostructure on a MUA SAM surface in a 0.1 M NaClO₄ solution. Inset is the overlay of cyclic voltammograms at different scan rates (100–800 mV).

electric field, especially for layers covered with redox active material. We observed that when a modulating potential (cyclic) is applied, the SPR signal responds to it and offers good measurement of the surface property pertinent to the deposited molecules. Upon a CV potential applied to the 1:1 FUT/MUA surface, there is an angular change in the SPR, which returns back to the baseline when the potential is returned (Fig. 6a). However, when there is no redox material present on the electrode surface, no SPR response was observed (Fig. 6b). Three contributing factors to the SPR response caused by cyclic voltammetry have been suggested, including a change in dielectric constant ($\Delta\epsilon$), a change in average thickness of the molecular layer (Δd), and/or a change in surface charge density of the electrode (Δq) [55,56]. In this case, it appears to be the change of charge density that has a large and direct impact on SPR signal due to the presence of a redox active film. It was observed that the SPR signal is proportional to the potential applied, indicating the method could be used to probe the extent of redox reaction on the surface. It also indicates that the polymer film has no blockage to the establishment of the double layer at the headgroup region. The deprotonation and protonation of ferrocene occurs rapidly, allowing for anionic electrolytes to

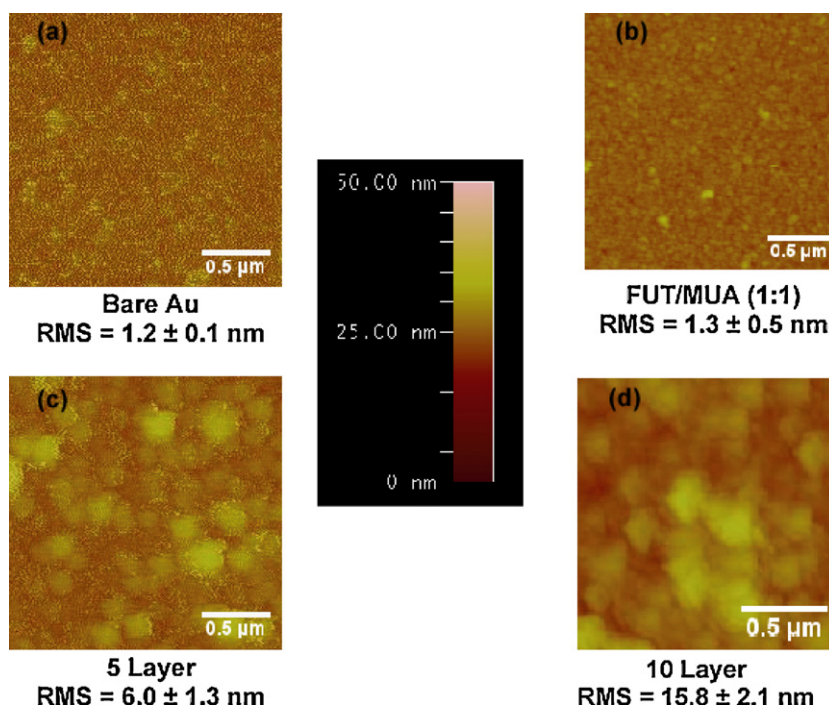


Fig. 7. Atomic force microscopy (AFM) images of (a) bare Au, (b) 1:1 FUT/MUA SAMs, (c) 5-layer build-up, and (d) 10-layer build-up.

move into and out of the porous polymer films (doping/dedoping) freely.

3.4. AFM and ellipsometry characterization

Further studies have been conducted using AFM and ellipsometry to confirm the ESPR results. The AFM image presented in Fig. 7a shows that the Au surface consists of flat grains, ~ 200 nm in size, and is characterized by the root-mean-square (rms) roughness of 1.2 ± 0.1 nm over an area of $5 \mu\text{m}^2$, which is in good agreement with previously reported Au substrates [26]. After incubation with 1:1 FUT/MUA the electrode surface becomes homogeneously covered with ferrocenyl-carboxylic alkanthiolates. The rms roughness for 1:1 FUT/MUA was found to be 1.3 ± 0.5 nm, with little structural heterogeneity observed on the surface. The ellipsometric measurement for the FUT/MUA monolayer had an effective film thickness of 1.5 ± 0.1 nm. The theoretical thickness of a $\text{COOH}(\text{CH}_2)_{10}\text{SAu}$ and $\text{Fc}(\text{CH}_2)_{10}\text{SAu}$ monolayer is found to be 1.5 and 1.7 nm, respectively. The theoretical and actual values are in good agreement with previous values found in the literature [26].

A 5-layer and a 10-layer polymer coating on 1:1 FUT/MUA were characterized by AFM, giving a rms roughness of 6.0 ± 1.3 and 15.2 ± 5.6 nm, respectively. The increase in roughness is a strong indicator that the surface is being built up by the deposition of polyelectrolytes that yield inhomogeneous structures. Ellipsometry measurements taking at layers of 1, 2, 4, 6, 8, and 10 yield thickness of 2.5 ± 0.3 , 3.3 ± 0.2 , 4.9 ± 0.2 , 6.3 ± 0.3 , 8.2 ± 0.3 , and 10.3 ± 0.5 nm, respectively. Close examination of these values shows that thickness by ellipsometry is much smaller than the value obtained through SPR estimation (for instance, 10.3 nm versus 12.6 nm for the 10-layer film). It is important to note that AFM and ellipsometry were performed in air, whereas all ESPR experiments were carried out in aqueous solutions. While the nanostructure in solution may exist in its fully hydrated form, exposure to air can lead to loss of water and thus shrinkage, and therefore a smaller thickness. The advantage of hydrated polyelec-

trolyte layer on the surface, as demonstrated here, is that it provides a greater number of “holes” for the ions to move in and out of freely, giving rise to a better movement of ions for compensating the charge imbalance due to ET, and thus presenting facile and unhindered redox chemistry on a covered surface.

4. Conclusions

Through a highly controlled surface procedure, an in-depth study of the polymer layer build-up and its effect on the electrochemical property of the covered redox moiety of a SAM film was performed. The LbL surface construction with PAH and PSS does not hinder the electron exchange to the redox active electrode. The highly porous films allow for the ionic counter charges to freely diffuse, which significantly enhances the ion conductivity of the films. The measured Γ_{Fc^+} reveals a full-coverage of a FUT/MUA monolayer with the quantity of surface-immobilized ferrocene, Γ_{Fc} , at $4.1(\pm 0.3) \times 10^{-10}$ mol cm^{-2} , and the current magnitude does not change after a ten layer polymer assembly. The electrochemical characterization shows an average peak separation of 30 ± 5.8 mV and the peak current is directly proportional to scan rate ($i_p \propto \nu$). The polyelectrolyte was able to completely adhere with great stability to the surface with no incubation needed. Overall, we have demonstrated a new three-dimensional nanoassembly interface with the desirable surface properties of facile electron transfer, free counter ion movement, and controlled multilayer build-up. This work opens avenues for a potentially multitude of new applications in the science of depositing thin polymer films over the surface of electron active electrodes such as, studying the mass transport of molecules across these films, thin film electrochemical detection, and creation of electroactive sites for biological detection. With the significantly increased capacity for hosting capture molecules on the polymer layer while remaining facile electron-transfer property, we next plan to build onto this multilayer system biological entities for sensing bacteria and viruses with a redox readout.

Acknowledgements

The authors would like to acknowledge financial support from NSF grant CHE-0719224. We thank Jeff Lefler for the help in the construction of the ESPR cell.

Appendix A. Supplementary data

Supplementary data associated with this article can be found, in the online version, at [doi:10.1016/j.electacta.2010.02.088](https://doi.org/10.1016/j.electacta.2010.02.088).

References

- [1] T.P. Cassagneau, J.H. Fendler, *Electrochem. Nanomater.* (2001) 247.
- [2] F.N. Crespilho, M.E. Ghica, C. Gouveia-Caridade, O.N. Oliveira, C.M.A. Brett, *Talanta* 76 (2008) 922.
- [3] R. Dronov, D.G. Kurth, H. Mohwald, F.W. Scheller, J. Friedmann, D. Pum, U.B. Sleytr, F. Lisdat, *Langmuir* 24 (2008) 8779.
- [4] F. Estrany, R. Oliver, E. Armelin, J.I. Iribaren, F. Liesa, C. Aleman, *Port. Electrochim. Acta* 25 (2007) 55.
- [5] Y. Gao, J.N.M. Shreeve, *J. Polym. Sci. A: Polym. Chem.* 43 (2005) 974.
- [6] H. Lee, Y.-C. Lin, H.-P.D. Shieh, J. Kanicki, *IEEE Trans. Electron. Dev.* 54 (2007) 2403.
- [7] W. Li, M. Xian, Z. Wang, C. Sun, M. Zhao, *Thin Solid Films* 386 (2001) 121.
- [8] J.B. Schlenoff, D. Laurent, H. Ly, J. Stepp, *Adv. Mater.* 10 (1998) 347.
- [9] N. Zhang, R. Schweiss, W. Knoll, *J. Solid-State Electrochem.* 11 (2006) 451.
- [10] P. Garcia-Vazquez, O.G. Morales-Saavedra, G. Pelzl, J.G. Banuelos, M.P. Carreon-Castro, *Thin Solid Films* 517 (2009) 1770.
- [11] T. Komikado, A. Inoue, K. Masuda, T. Ando, S. Umegaki, *Thin Solid Films* 515 (2007) 3887.
- [12] S.-S. Lee, J.-D. Hong, C.H. Kim, K. Kim, J.P. Koo, K.-B. Lee, *Macromolecules* 34 (2001) 5358.
- [13] J. Seo, J.L. Lutkenhaus, J. Kim, P.T. Hammond, K. Char, *Langmuir* 24 (2008) 7995.
- [14] S.A. Yeroshina, N.K. Ibrayev, S.E. Kudaibergenov, F. Rullens, M. Devillers, A. Laschewsky, *Thin Solid Films* 516 (2008) 2109.
- [15] M. Yu, J. Zhang, D. Li, Q. Meng, W. Li, *Appl. Surf. Sci.* 253 (2007) 3276.
- [16] D.R. Talham, T. Yamamoto, M.W. Meisel, *J. Phys.: Condens. Matter* 20 (2008) 184006.
- [17] R.C. Jaeger, *Introduction to Microelectronic Fabrication*, in: G.W. Neudeck, R.F. Pierret (Eds.), Vol. V in the modular series on Solid State Devices, 2nd ed., Prentice Hall, Upper Saddle River, NJ, 2002.
- [18] G. Decher, *Science* 277 (1997) 1232.
- [19] P. Bertrand, A. Jonas, A. Laschewsky, R. Legras, *Macromol. Rapid Commun.* 21 (2000) 319.
- [20] K. Ariga, J.P. Hill, Q. Ji, *Phys. Chem. Chem. Phys.* 9 (2007) 2319.
- [21] G. Decher, Y. Lvov, J. Schmitt, *Thin Solid Films* 244 (1994) 772.
- [22] Y. Lvov, H. Haas, G. Decher, H. Moehwald, A. Mikhailov, B. Mchedlishvili, E. Morgunova, B. Vainshtein, *Langmuir* 10 (1994) 4232.
- [23] A. Ulman, *Chem. Rev.* 96 (1996) 1533.
- [24] L. Shen, H. Hu, *Biomacromolecules* 6 (2005) 1475.
- [25] J.C. Love, L.A. Estroff, J.K. Kriebel, R.G. Nuzzo, G.M. Whitesides, *Chem. Rev.* 105 (2005) 1103.
- [26] L.L. Norman, A. Badia, *Langmuir* 23 (2007) 10198.
- [27] N. Zhang, R. Schweiss, Y. Zong, W. Knoll, *Electrochim. Acta* 52 (2007) 2869.
- [28] R. Kurita, Y. Yokota, A. Ueda, O. Niwa, *Anal. Chem.* 79 (2007) 9572.
- [29] B.J. Privett, J.H. Shin, M.H. Schoenfish, *Anal. Chem.* 80 (2008) 4499.
- [30] J. Heinze, *Angew. Chem.* 96 (1984) 823.
- [31] J.R. Sambles, G.W. Bradbery, F. Yang, *Contemp. Phys.* 32 (1991) 173.
- [32] E.A. Smith, R.M. Corn, *Appl. Spectrosc.* 57 (2003) 320A.
- [33] A. Baba, P. Taranekar, R.R. Pannapati, D. Patton, W. Knoll, R.C. Advincula, *Polym. Preprints* 47 (2006) 1080.
- [34] S. Sriwichai, A. Baba, S. Deng, C. Huang, S. Phanichphant, R.C. Advincula, *Langmuir* 24 (2008) 9017.
- [35] W. Hu, C.M. Li, X. Cui, H. Dong, Q. Zhou, *Langmuir* 23 (2007) 2761.
- [36] A.J. Bard, L.R. Faulkner, *Electrochemical Methods: Fundamentals and Applications*, Wiley, New York, 2001.
- [37] T. Ohtsuka, Y. Sato, K. Uosaki, *Langmuir* 10 (1994) 3658.
- [38] A.G. Brolo, R. Gordon, B. Leathem, K.L. Kavanagh, *Langmuir* 20 (2004) 4813.
- [39] M. An, J.-D. Hong, *Thin Solid Films* 500 (2006) 74.
- [40] J.B. Schlenoff, S.T. Dubas, *Macromolecules* 34 (2001) 592.
- [41] E.D. Palik, *Handbook of Optical Constants of Solids*, Academic Press, 1998.
- [42] S. Ye, Y. Sato, K. Uosaki, *Langmuir* 13 (1997) 3157.
- [43] Y.-Y. Luk, L. Abbott Nicholas, *Science* 301 (2003) 623.
- [44] T. Hasunuma, S. Kuwabata, E. Fukusaki, A. Kobayashi, *Anal. Chem.* 76 (2004) 1500.
- [45] X. Yao, M. Yang, Y. Wang, Z. Hu, *Sens. Actuators, B* 122 (2007) 351.
- [46] B. Seiwert, U. Karst, *Anal. Bioanal. Chem.* 390 (2008) 181.
- [47] S.S. Shiratori, M.F. Rubner, *Macromolecules* 33 (2000) 4213.
- [48] D. Yoo, S.S. Shiratori, M.F. Rubner, *Macromolecules* 31 (1998) 4309.
- [49] J.-B. Raoof, R. Ojani, S. Rashid-Nadimi, *Electrochim. Acta* 53 (2008) 7261.
- [50] K. Gibasiewicz, M. Pajzderska, *J. Phys. Chem. B* 112 (2008) 1858.
- [51] A.-E.F. Nassar, W.S. Willis, J.F. Rusling, *Anal. Chem.* 67 (1995) 2386.
- [52] S.A. Merchant, D.T. Glatzhofer, D.W. Schmidtke, *Langmuir* 23 (2007) 11295.
- [53] B.-Y. Chang, E. Ahn, S.-M. Park, *J. Phys. Chem. C* 112 (2008) 16902.
- [54] L. Rassaei, M. Sillanpaae, F. Marken, *Electrochim. Acta* 53 (2008) 5732.
- [55] X. Kang, Y. Jin, G. Cheng, S. Dong, *Langmuir* 18 (2002) 1713.
- [56] A. Baba, M.-K. Park, R.C. Advincula, W. Knoll, *Langmuir* 18 (2002) 4648.